International Journal of Hydrogen Energy 87 (2024) 159–170

Contents lists available at ScienceDirect

International Journal of Hydrogen Energy

journal homepage: www.elsevier.com/locate/he

An analytical methodology to maximize the fuel cells system efficiency using optimal cathodic pressure and flow rate

Alessandro d'Adamo *, Lorenzo Martoccia, Fabio Berni, Sebastiano Breda

Dipartimento di Ingegneria "Enzo Ferrari", Università degli Studi di Modena e Reggio Emilia, Modena, Italy

ARTICLE INFO

Handling Editor: Dr C O Colpan

ABSTRACT

Hydrogen fuel cells are one of the main solutions for power generation, combining the decarbonization urgency with a high energy conversion efficiency. In this context, the efficiency of a fuel cell system (FCS) is a key factor to maximize, as conversion efficiency improvements are beneficial to both reduce the hydrogen consumption and increase the power density. In this context, the design of the air supply system allows to operate the cathode at various pressures and flow rates, potentially increasing the cell efficiency although critically raising the power demand on the same system. Hence, its optimization is far from trivial and requires a solid model-based analysis.

In this study an analytical methodology is presented to quantify the efficiency variation in FCS operating at various pressure and/or flow rates using supercharging devices. The accompanying MATLAB script is distributed under the FAIR (Findable, Accessible, Interoperable, Reusable) guidelines upon request, and it allows an *a priori* evaluation of the conditions for maximum FCS efficiency. The methodology is of general use, and it is demonstrated on a wide range of air flow rates ($\lambda_c = 1.2 - 10.0$) and pressure ($p_c = 1.0 - 5.0\ bar$) using data from two literature cells, and with high and low efficiency turbomachinery. Results indicate that the maximum FCS efficiency is generally obtained for high stoichiometric factors ($\lambda_c = 5.0 - 6.8$) and low-to-moderate cell backpressure ($p_c = 1.0 - 1.3\ bar$) when no pressure losses are included in the air admission line. When these are accounted for, the same methodology indicates a lower stoichiometric factor ($\lambda_c = 2.2 - 3.0$) and a slightly higher cell backpressure ($p_c = 1.2 - 2.0\ bar$). Despite numbers vary with specific systems, the methodology is both analytically based and highly general, hence scalable to any FCS. The presented model relevantly offers a model-based guidance to design the air supply line for maximum system efficiency, thus reinforcing the engineering of fuel cell systems.

1. Introduction

Fuel cells are electrochemical energy converters, allowing a direct conversion of reactants chemical energy into useful electrical energy, thus circumventing the inherent thermodynamic limitations of thermal-based converters, e.g. gas turbines, internal combustion engines, burners, etc [1,2]. This characteristic allows higher thermodynamic energy conversion efficiency than combustion devices. When considering also faster energy refill operation and higher power density than battery systems, combined with the inherent modularity, rapid response time, low-temperature operation and absence of pollutants emissions for hydrogen-fuelled Polymeric Electrolyte Membrane Fuel Cell (PEMFC), it is clear how such technology is considered a key enabler to jointly decarbonize and increase the efficiency of a wide spectrum of power generation systems, from the transportation sector to the stationary power supply [3,4], as shared by recent reviews on the status and perspective of the fuel cells status and advances, with focus on the transportation industry [5–9].

In typical fuel cells systems (FCS), several auxiliaries are needed to support the power generation process, e.g. cooling sub-system for thermal management, hydrogen, and pressurized air supply lines. At the cell level, oxygen-containing air and hydrogen are the necessary reactants for the electrochemical reactions developing in PEMFCs, producing water and heat and requiring a careful interplay of functional parts and materials (i.e. diffusion media, conduction through the solid phase, diffusion-driven fluid transport, electrolyte resistance minimization, etc.), whose fundamental aspects and the engineering details that made the PEM type a leading fuel cell architecture are resumed in Refs. [10,11]. At a system level, the air flow rate for the cathodic reaction is the most critical one from an energy perspective, as the

* Corresponding author. Dipartimento di Ingegneria "Enzo Ferrari", Università degli Studi di Modena e Reggio Emilia, Via P. Vivarelli 10, 41125, Modena, Italy.
E-mail address: alessandro.dadamo@unimore.it (A. d'Adamo).

https://doi.org/10.1016/j.ijhydene.2024.09.018
Received 26 June 2024; Received in revised form 5 August 2024; Accepted 2 September 2024
Available online 7 September 2024

oxygen-containing air is typically taken from the humid ambient and an air compressor is used to realize both the desired pressure and air flow rate. Several compressor types and layouts are possible, with centrifugal, scroll and screw compressor being the dominant choices [12,13]. The cathodic air flow rate is quantified by the stoichiometric factor (λ_c), defined as the effective air flow rate with respect to the oxygen flux converted in electric current. The high pressure and high flow rate operation increases the cell power generation, resulting in higher stack power density. This allows to minimize the number of cells for a given output power, together with the weight, volume, and cost. However, as the power demand to drive the compressor burdens on the PEMFC itself, a careful choice of the pressure and λ_c is mandatory to limit the power absorption, and similar conclusions apply also in case a turbine (expander) is added to recover part of the pressurized exhaust gas energy, creating an electrically assisted supercharger.

Focusing on the cell level, the efficiency of PEMFCs is known to increase both under high pressure operation and elevated λ_c: the former aspect is motivated by the increase in open-circuit voltage (OCV) potential as per the Nernst equation [14], whereas the latter is beneficial in over-delivering oxygen to the cathodic catalyst layer, thus balancing the oxygen partial pressure decrease due to reduction reaction. A high air flow rate is also positive in suppressing the concentration overpotential and contrasting the flooding onset. Therefore, the analysis of cell performance indicates that both air pressure and flow rate should be synergically increased to maximize the efficiency. Examples are the studies from Santarelli et al. [15] and Wang et al. [16], confirming the beneficial high-pressure operation up to 3.0 *bar* on small PEMFCs, although their laboratory studies did not include the power balance for the air compressor. Moving to PEMFC systems, Lu et al. [14] highlighted that high-pressure operation introduced the positive aspect of increasing the membrane water content via enhanced relative humidity, reducing the cell resistance. When a simple power balance for an air compressor was added to their experimental and modelling study, the optimal range for cell pressure was restricted to $1.5 - 2.0$ *bar* from the wider spectrum of beneficial conditions for the cell operation (up to 2.5 *bar*), whereas a uniform $\lambda_c = 2.0$ was used. A similar indication of intermediate cell pressure was reported by Kim et al. [17] in a PEMFC system simulation study, indicating a maximum system efficiency in the range $1.7 - 3.0$ *bar* for $\lambda_c = 2.0$. In Ref. [18] a combined pressure and λ_c study was carried out on a 30 kW PEMFC stack for automotive use, using empirical fitting models for both the cell and the compressor performance, and obtaining similar conclusions albeit limited to the investigated case. Different conclusions are reported by Qin et al. [19], where an indication of "*no compression*" (operating pressure equal to 1.2 *bar*) at $\lambda_c = 2.0$ was reported, again based on fitted equations for the compressor in use and critically reporting a compressor efficiency lower than 0.45, which is believed to largely contribute to the observed results. Another remarkable study was conducted by Chen et al. [20], where a 3D-CFD for as PEMFC and a compressor map for a 30-kW automotive stack system were used to indicate an air excess ratio lower than $\lambda_c = 4.0$ and a cathodic pressure lower than 1.7 *bar* as best operating conditions, highlighting an inverse proportionality between the operating pressure and λ_c for optimal operation for the best efficiency. Martinez-Boggio et al. [21] modelled several air admission layouts using genetic algorithms, identifying the turbine-assisted layout as the best solution, using a commercial software for the genetic algorithm analysis. As for the effect of λ_c, Santarelli et al. [22] tested values in the range 1.3–4.5 on a laboratory 3.5 kW PEMFC stack at ambient pressure, underlying the importance to operate with $\lambda_c \geq 2.0$ and qualitatively estimating a system efficiency increase when the power demand for a compressor was included in the analysis. Ge et al. [23] proposed an optimization study of air excess ratio and cathodic pressure for a 65 kW FC bus, indicating the relevance of low-pressure and high air excess ratio operation to maximize the system efficiency, although results are only discussed for the investigated application.

Therefore, a delicate optimization problem arises in terms of cathodic pressure and λ_c, as the choice of operating conditions and auxiliaries could lead either to an overall system efficiency increase or to the opposite conclusion. The primary role of the system efficiency as a key performance indicator, and the possibility to largely increase or reduce it when coupling a PEMFC with a supercharger, motivate the urgency in developing a robust model-based methodology to unambiguously identify the optimal operating pressure and air flow rates, hence right-sizing the air admission line [21]. Unfortunately, to the extent of the authors' knowledge such methodology is missing in the specialized literature, and the identification of the optimal pressure and flow rate values is often based on experience, optimization software, or on case-by-case measurements (*a posteriori*), critically limiting the generality of the conclusions and marginally contributing to a broader engineering knowledge.

The main aim of the present study is the development of an *a priori* analytical methodology to select the pressure and λ_c values to maximize the FCS efficiency. In the first part, the analytical derivation of the procedure to identify the optimal ranges for the steady-state cathodic pressure and air flow rates is presented, based on simple cell and supercharger models. In the second part, this is applied to four realistic PEM-type FCS: the data of two MEAs tested at the Joint Research Center for benchmarking and validation purposes ([24,25]) are coupled with high- and low-efficiency (HE and LE, respectively) supercharging systems. The FCS efficiency evaluated both at minimum supercharging power demand and at conditions for zero-gradient MEA studies is compared with that identified by the presented model, indicating in all cases a relevant FCS efficiency improvement. The study is implemented in a MATLAB script which will be made available upon request to the authors. The discussion of results demonstrates the importance of limiting the cell operating pressure and the need to realize a sufficiently high λ_c, relevantly providing an analytical and general methodology scalable to any fuel cell system. Moreover, it provides a quantitative answer to the ever-present interest in very high pressure levels or flow rate, showing their detrimental effect on the FCS efficiency when operated in combination with high flow rates. The relevance of the study lies in filling the knowledge gap in guiding in the selection of the optimal air pressure and flow rate values, offering a wide-use support for the coupling of supercharger and PEMFC to maximize the system efficiency. The novelty of the presented model is its generic derivation which allows its application to any PEMFC system software or R&D workflow, fulfilling the main objective to provide a solid methodology for the design of the air admission line of FCS for maximum efficiency.

2. Methodology

The study presents an equation-based methodology to predict the performance of a supercharged FCS, where the operating pressure and the air flow rate are considered two degrees of freedom for optimal system operation. The analysis is carried out to be as general as possible to maximize its scalability, and two PEMFC polarization curves from literature alongside typical data for auxiliaries are used for a demonstration study on multiple cases. The conditions of interest (i.e. the cell backpressure and the cathodic stoichiometric factor, hereafter p_c and λ_c) constitute the two unknown variables to design the FC supercharging system, whose selection has profound implications on the system efficiency as they affect both the power demand for supercharging and the cell power generation in a complex way. The next sections will describe the modelling approaches for the cell, the compressor, the turbine, and their combined operation (supercharger) for various p_c and λ_c levels. The model has been implemented in a MATLAB routine which will be made available upon request to the authors.

2.1. Modelling of fuel cell performance

The fuel cell performance is synthetized by the current density-voltage (polarization) curve, typically obtained via empirical fitting of

experimental data or via analytical formulations [26]. The cell potential (E_{cell}) at given conditions is obtained by the current-independent open-circuit voltage (E_{OCV}), reduced by the effect of fuel crossover and internal currents (hence referred to as "mixed potential", E^*_{OCV}) and reduced by the overpotentials as in Eq. (1).

$$E_{cell}(p_c, i) = E^*_{OCV} - \eta_{act} - \eta_{ohm} - \eta_{conc} \tag{1}$$

The activation, ohmic and concentration overpotentials are modelled as $\eta_{act} = \frac{R\,\overline{T}_c}{\alpha\,F}\,ln\left(\frac{i}{i_0}\right)$, $\eta_{ohm} = r_{cell}\,i$ and $\eta_{conc} = m\,e^{n\,i}$, respectively, with $\overline{T}_c$ being the average cell temperature, α the charge transfer coefficient, i_0 the exchange current density, r_{cell} the total cell resistance, and m and n empirical fitting coefficients for concentration losses [1].

The operating pressure influences the polarization curve in terms of E^*_{OCV} and i_0, with the ambient pressure as the reference condition for both quantities ($E^*_{OCV,amb}$ and $i_{0,amb}$, respectively). The former aspect is accounted for by the Nernst equation leading to ΔE^*_{OCV} as in Eq. (2), whereas the latter is calculated based on the relationship from Ref. [2] and reported in Eq. (3). Both factors indicate an increase in the cell efficiency for higher p_c, motivated by a higher E^*_{OCV} and a lower activation overpotential at higher pressures due to increased i_{0,p_c}.

$$\Delta E^*_{OCV} = \frac{R\,\overline{T}_c}{4\,F}\,ln\left(\frac{p_c}{p_{amb}}\right) \tag{2}$$

$$i_{0,p_c} = i_{0,amb}\left(\frac{p_c}{p_{amb}}\right)^{\gamma} \tag{3}$$

The cathodic λ_c indirectly modifies the polarization curve, being all the overpotentials explicitly dependent only on i, and not on λ_c. However, λ_c is a common operating index for PEMFC systems, hence of relevant practical interest. When operating at very high flow rates ($\lambda_c \rightarrow \infty$), an abundant and uniform oxygen concentration over the entire cell area is assumed; however, the use of lower λ_c is more common due to the critical power demand of the supercharger. The effect of finite λ_c values on the cell operation was modelled by the f_{λ_c} function proposed by Kulikovsky in Ref. [27] and reported in Eq. (4), which is adopted in the present model. This function indicates an asymptotic gain in cell efficiency for $\lambda_c \rightarrow \infty$ operation, due to the attenuation of activation and concentration overpotentials, whereas the finite oxygen availability over the cell MEA increases the same overpotentials at low λ_c. The effect is particularly relevant at high i, in line with the experimental outcomes in Ref. [22]. The combined effect of p_c and λ_c is expressed by Eq. (5), and both factors should be increased for optimal cell efficiency; however, they also raise the power demand for supercharging to generate such conditions, as will be discussed in the next section, thus hindering a trivial selection of maximum cathodic pressure and flow rate operation. Finally, the cell thermodynamic efficiency (η_{cell}) and gross power (P_{cell}) for varying p_c and λ_c are calculated as in Eqs. (6) and (7), respectively, with E_{th} being the thermoneutral potential based on hydrogen higher heating value.

$$f_{\lambda_c} = -\lambda_c\,ln\left(1 - \frac{1}{\lambda_c}\right) \tag{4}$$

$$E_{cell}(p_c, \lambda_c) = E^*_{OCV,amb} + \Delta E^*_{OCV} - \frac{R\,\overline{T}_c}{\alpha\,F}\,ln\left(\frac{f_{\lambda_c}\,i}{i_{0,p_c}}\right) - r_{cell}\,f_{\lambda_c}\,i - m\,e^{n\,f_{\lambda_c}\,i} \tag{5}$$

$$\eta_{cell}(p_c, \lambda_c) = \frac{E_{cell}(p_c, \lambda_c)}{E_{th}} \tag{6}$$

$$P_{cell}(p_c, \lambda_c) = E_{cell}(p_c, \lambda_c)\,i\,A_{MEA} \tag{7}$$

2.2. Modelling of compressor and turbine

The air compressor increases the pressure of the humid ambient air to the cell operating pressure. In this study, the pressure at cell outlet (backpressure, p_c) is considered as the cell operating pressure. The calculation of the compressor power demand requires the knowledge of the desired pressure at cell inlet (p_c^{in}), which is obtained adding the pressure losses in the cell flow (e.g., concentrated and distributed losses in channels) to the cell backpressure. This can be expressed as $p_c^{in} = p_c + \Delta p_{cell}$, with the air flow velocity at cell inlet (v_{in}) and Δp_{cell} calculated as in Eqs. (8) and (9) for a parallel channel flow field [28–30], using the air density and Reynolds number at cell inlet (ρ_{in} and Re_{in}), the channel length and hydraulic diameter (L_{ch} and D_{ch}), the cross-sectional channel area (A_{ch}), the MEA portion interested by the air flow of a single channel ($A_{MEA,ch}$, calculated as the product of channel length and twice the channel width), a concentrated loss coefficient depending on the inlet/outlet duct design (K_L), and the dry air molar mass (M_{air}). The water mass fraction at inlet ($Y_{w,c}$) is calculated based on the assigned relative humidity value provided by a humidifier installed after the compressor outlet section, which is assumed as a design input. Considering a parallel channel arrangement, the pressure loss calculated for the flow in a single channel is the same as that experienced by the total flow rate through the channels assembly in the bipolar plate, i.e. $\Delta p_{cell}(p_c, \lambda_c)$.

$$v_{in} = \frac{1}{\rho_{in}\,A_{ch}}\left(\frac{1}{1 - Y_{w,c}}\,\frac{\lambda_c}{0.21}\,\frac{M_{air}}{4\,F}\right) i\,A_{MEA,ch} \tag{8}$$

$$\Delta p_{cell}(p_c, \lambda_c) = \left[\frac{59.62}{Re_{in}}\,\frac{L_{ch}}{D_{ch}} + K_L\right]\rho_{in}\frac{v_{in}^2}{2} \tag{9}$$

The relationship in Eq. (9) indicates that a high p_c and λ_c operation inevitably leads to elevated pressure losses in the cell, due to the higher gas density and flow velocity, ultimately adding an additional request to the pressure level to be generated by the air compressor. The resulting pressure loss is used to calculate the compressor outlet pressure (p_c^{in}), hence the power absorption (P_C) [2] as in Eq. (10), with $\eta_{i,c}$ and $\eta_{m,c}$ being the internal and mechanical efficiency of the compressor, T_{amb} the ambient air, c_p the air isobaric specific heat, γ the ratio of air specific heats, and where the negative sign is used to remark the power request. The compressor efficiencies are modelled as constant values under the hypothesis of steady-state conditions.

$$P_C = -\,\dot{m}_{air}\,c_p\,\frac{T_{amb}}{\eta_{i,C}\,\eta_{m,C}}\left[\left(\frac{p_c^{in}}{p_{amb}}\right)^{\frac{\gamma-1}{\gamma}} - 1\right] \tag{10}$$

The humid air flow rate for the compressor in Eq. (10) can be expressed as a function of the cathodic stoichiometric factor (λ_c) and of the cell current density (i) as in Eq. (11):

$$\dot{m}_{air} = \frac{1}{1 - Y_{w,amb}}\,\frac{\lambda_c}{0.21}\,\frac{M_{air}}{4\,F}\,i\,A_{MEA} \tag{11}$$

Introducing the terms $\xi_1 = \frac{1}{1-Y_{w,amb}}\,\frac{\lambda_c}{0.21}\,\frac{M_{air}}{4\,F}$ and $\Gamma_C = c_p\,\frac{T_{amb}}{\eta_{i,C}\,\eta_{m,C}}$ for notation compactness, Eq. (11) reduces to Eq. (12), and Eq. (10) is manipulated into Eq. (13), expressing the compressor power demand as a function of p_c and λ_c, i.e. $P_C(p_c, \lambda_c)$:

$$\dot{m}_{air} = \xi_1\,i\,A_{MEA} \tag{12}$$

$$P_C(p_c, \lambda_c) = -\,\xi_1\,i\,A_{MEA}\,\Gamma_C\left[\left(\frac{p_c + \Delta p_{cell}}{p_{amb}}\right)^{\frac{\gamma-1}{\gamma}} - 1\right] \tag{13}$$

In a similar way, the power harvested by the turbine (P_T) is calculated as in Eq. (14) [2], where the positive sign indicates a useful power and with $\eta_{i,T}$ and $\eta_{m,T}$ being the internal and mechanical efficiency of the turbine, modelled as constant values under the hypothesis of steady-state operation. In this study, the turbine is assumed to be mechanically coupled with the compressor, forming a turbocharging unit.

$$P_T = \dot{m}_{out} c_p T_c^{out} \eta_{i,T} \eta_{m,T} \left[1 - \left(\frac{p_{amb}}{p_c}\right)^{\frac{\gamma-1}{\gamma}}\right] \tag{14}$$

The flow rate at cell outlet ($\dot{m}_{out}$) is composed by the sum of the flow rate at cell inlet increased by the water flow rate produced by the oxygen reduction in the cell ($\dot{m}_{w,react}$, Eq. (15)), the water flow rate from the cathode-directed net drag ($\dot{m}_{w,drag}$, Eq. (16)), and the water flow rate provided by the cell humidifier installed after the compressor outlet section ($\dot{m}_{w,hum}$, Eq. (17)). The net drag coefficient (r_d) is used in Eq. (16) to express the net rate of water transported in the membrane, experimentally measured in Ref. [31] and bundling the cathode-directed electro-osmotic drag and the water back-diffusion. In the limit that all the produced water is evaporated and removed from the CL region, Eq. (18) expresses the flow rate at turbine inlet ($\dot{m}_{out}$):

$$\dot{m}_{w,react} = \frac{M_w}{2F} i A_{MEA} \tag{15}$$

$$\dot{m}_{w,drag} = r_d \frac{i A_{MEA}}{F} M_w \tag{16}$$

$$\dot{m}_{w,hum} = \dot{m}_{air} \left(\frac{1 - Y_{w,amb}}{1 - Y_{w,c}} - 1\right) \tag{17}$$

$$\dot{m}_{out} = \xi_1 \, i A_{MEA} + \dot{m}_{w,react} + \dot{m}_{w,drag} + \dot{m}_{w,hum} \tag{18}$$

Knowing the temperature increase in the cell ΔT_{cell} from direct measurements, as in Ref. [32], or using calculations so that $T_c^{out} = T_c^{in} + \Delta T_{cell}$ and introducing the term $\Gamma_T = c_p T_c^{out} \eta_{i,T} \eta_{m,T}$ and $\xi_2 = \frac{M_w}{2F}$ for notation compactness, Eq. (14) is manipulated into Eq. (19) and it expresses the turbine power recovery (positive sign) as a function of p_c and λ_c, i.e. $P_T(p_c, \lambda_c)$:

$$P_T(p_c, \lambda_c) = i A_{MEA} \, (\xi_1 + \xi_2) \, \Gamma_T \left[1 - \left(\frac{p_{amb}}{p_c}\right)^{\frac{\gamma-1}{\gamma}}\right] \tag{19}$$

Finally, the supercharging system is composed by the assembly of compressor and turbine; hence, the global power value (P_{SC}) is given as in Eq. (20) by balance of the contributions of compressor, turbine, and parasitic power absorption. The latter considers that even in idle conditions the supercharger must be operated at a minimum rotational speed, and that other minor power absorption are required for the system operation (e.g., the coolant pump, etc.), ultimately requiring a power absorption ($P_{par} < 0$). The numerically dominant contribution is the compressor power, leading to global net power demand (i.e. negative) for supercharging for varying p_c and λ_c. This will be supplied by the cell electric power, hence representing a parasitic loss, and leading to a potentially severe power penalty of the fuel cells system, thereby motivating a careful selection of (p_c, λ_c) operating conditions. Considering that the supercharger needs to be electrically assisted (motorized turbocompressor), the term "supercharging" is preferred to "turbocharging". Finally, the efficiency of an electric motor (η_{mot}) is considered, and net power of the FCS is obtained as in Eq. (20), i.e. $P_{SC}(p_c, \lambda_c)$.

$$P_{SC}(p_c, \lambda_c) = \frac{P_C(p_c, \lambda_c) + P_T(p_c, \lambda_c) + P_{par}}{\eta_{mot}} \tag{20}$$

2.3. Analysis of fuel cell system

The power of an FCS indicates the net power output of the fuel cell system as in Eq. (21), quantifying the reduction of the cell gross power output due to the supercharging system demand as a function of p_c and λ_c. In the same way, the efficiency of the auxiliaries (η_{aux}) can be expressed as the ratio of the gross over net power output, as in Eq. (22), leading to the FCS efficiency (η_{FCS}, Eq. (23)) as the main indicator of efficient energy conversion. The maximization of $\eta_{FCS}(p_c, \lambda_c)$ from a mathematical *a priori* evaluation constitutes the backbone of the presented methodology, which will be demonstrated on two realistic cases in the next section.

$$P_{FCS}(p_c, \lambda_c) = P_{cell}(p_c, \lambda_c) + P_{SC}(p_c, \lambda_c) \tag{21}$$

$$\eta_{aux}(p_c, \lambda_c) = \frac{P_{FCS}(p_c, \lambda_c)}{P_{cell}(p_c, \lambda_c)} \tag{22}$$

$$\eta_{FCS}(p_c, \lambda_c) = \eta_{cell}(p_c, \lambda_c) \, \eta_{aux}(p_c, \lambda_c) \tag{23}$$

3. Results

3.1. Cell data and conditions of interest

The methodology is demonstrated on two cells and using two supercharging models, representative of high- and low-efficiency, and all the input data used are reported in Table 1. All the values are chosen to be as representative as possible of realistic fuel cells systems, reinforcing the important aim of the methodology, i.e. a general applicability to any FCS.

The data published by the Joint Research Centre (JRC) on two MEAs are used as representative cell models. In coherence with [24,25], these are named MEA1 (28 μm thickness) and MEA2 (18 μm thickness), respectively. Both MEAs were tested on a single serpentine and on a parallel channel hardware, this last aiming at realizing optimal conditions for MEA testing and validation studies and called Zero-Gradient Cell (JRC ZERO∇CELL). Such conditions were obtained operating the cell at $p_c = 2.3\ bar$ and $\lambda_c = 10.0$, and they were explicitly derived to ensure a uniform reactants delivery to the entire MEA area for membrane studies, not aiming at increasing the system efficiency. This zero-gradient operating condition will be hereafter referred to as ZG. The experimental polarization curves for MEA1 and MEA2 and the two fitting models using Eq. (5) for the same (p_c, λ_c) values are reported in Fig. 1. This includes also the modified cell polarization curves for MEA1 and MEA2 for the minimal parasitic loss condition ($p_c = 1.0\ bar, \lambda_c = 1.2$), still calculated using Eq. (5) and showing the expected overpotentials increase. All the fitting coefficients used for Eq. (5) to reproduce the experimental data from Refs. [24,25] (i.e., i_0, r_{cell}, m, n) are resumed in Table 1. The variation of the activation and concentration overpotentials are reported in Fig. 2 for the MEA1 case, where it is evident the extent of loss attenuation as modelled by Eqs. (3) and (4) and

Table 1
Input data used for model results.

Data	Unit	Comment
$\gamma = 1.4$	–	Ratio of air specific heats
$c_p = 1000$	$\frac{J}{kg\,K}$	Isobaric air specific heat
$\eta_{i,C} = 0.75 - 0.55$	–	Compressor internal efficiency (HE - LE)
$\eta_{m,C} = 0.98$	–	Compressor mechanical efficiency
$\eta_{i,T} = 0.85 - 0.65$	–	Turbine internal efficiency (HE - LE)
$\eta_{m,T} = 0.98$	–	Turbine mechanical efficiency
$\eta_{mot} = 0.9 - 0.8$	–	Electric motor efficiency (HE - LE)
$\alpha = 1.0$	–	Charge transfer coefficient
$p_{amb} = 1 \times 10^5$	Pa	Ambient pressure
$T_{amb} = 298$	K	Ambient temperature
$T_c^{in} = 353$	K	Cell inlet temperature
$\Delta T_{cell} = 10$	K	Temperature increase in the cell
$D_h = 1$	mm	Channel hydraulic diameter
$A_{MEA} = 250$	cm^2	Membrane and electrode assembly active area
$i_{0,amb} = 1.25 \times 10^{-6}$	$\frac{A}{cm^2}$	Cathodic exchange current density at ambient pressure
$r_{cell} = 0.09 - 0.06$	$\Omega\,cm^2$	Total cell resistance (MEA1 – MEA2)
$m = 1 \times 10^{-2} - 5 \times 10^{-4}$	V	1st coefficient for concentration overpotential fit (MEA1 – MEA2)
$n = 0.9 - 1.15$	$\frac{cm^2}{A}$	2nd coefficient for concentration overpotential fit (MEA1 – MEA2)
$P_{idle} = -12$	W	Parasitic power absorption

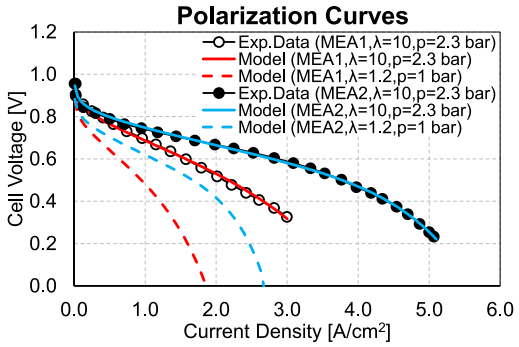

Fig. 1. Cell polarization curves for MEA1 and MEA2 from experiments ([24, 25]) and fitted using Eq. (5) for $p_c = 2.3\ bar$ and $\lambda_c = 10.0$ and for the minimal parasitic loss condition ($p_c = 1.0\ bar$, $\lambda_c = 1.2$).

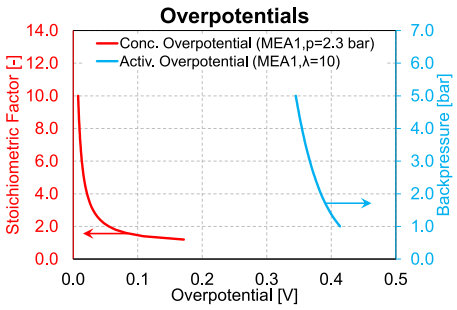

Fig. 2. Cell overpotentials for MEA1: concentration overpotential based on Eq. (4) as a function of λ_c (left y-axis), and activation overpotential based on Eq. (3) as a function of p_c (right y-axis).

made possible by the operation at high pressure and stoichiometric factor.

The evaluated conditions for the methodology demonstration are those of highest interest both for p_c and λ_c. As for the cathodic pressure, a minimum backpressure equal to the ambient one ($p_c = 1.0\ bar$) is assumed as a minimum limit for air delivery power demand to contrast only the pressure losses in the cell, whereas the maximum backpressure is set to $p_c = 5.0\ bar$ and a stepping of 0.1 *bar* is chosen (41 values). The cathodic stoichiometric flow rate is evaluated from $\lambda_c = 1.2$, considered as a minimum value for starvation-limited cell operation, to $\lambda_c = 10.0$, with a stepping of $\lambda_c = 0.2$ (45 values). A full factorial set of 1845 conditions are simulated using an in-house developed MATLAB program. The cell efficiency and power output at varying p_c and λ_c are calculated as in Eqs. (6) and (7), respectively, and an increase in both factors would be synergically beneficial both for cell efficiency and electric power. In Fig. 3 the cell efficiency and power iso-contours are reported for MEA1 at medium ($i = 0.8A/cm^2$) and high ($i = 1.5A/cm^2$) current density, confirming that, from a cell perspective, both pressure and air flow rate should be maximized, hence locating the optimal operating point in the top-right corner of Fig. 3, i.e. at the highest possible p_c and λ_c. However, this ignores the power demand to realize such conditions, whose impact will be quantified in the next section.

3.2. Results of supercharging modelling

The supercharging system requires a net power use ($P_{SC} < 0$) under all tested conditions. Introducing realistic input data resumed in Table 1, the compressor, turbine, and supercharger power are reported in Fig. 4 for low ($\lambda_c = 1.6$) and medium ($\lambda_c = 3.0$) stoichiometric factors for the HE case. As expected, both the minimum power demand for compression (Fig. 4-a/b) and the minimum power recovery from turbine (Fig. 4-c/d) are predicted for the lowest (p_c, λ_c) values (i.e., bottom-left corner), hereafter named Minimal Power Demand (MPD) condition, the opposite

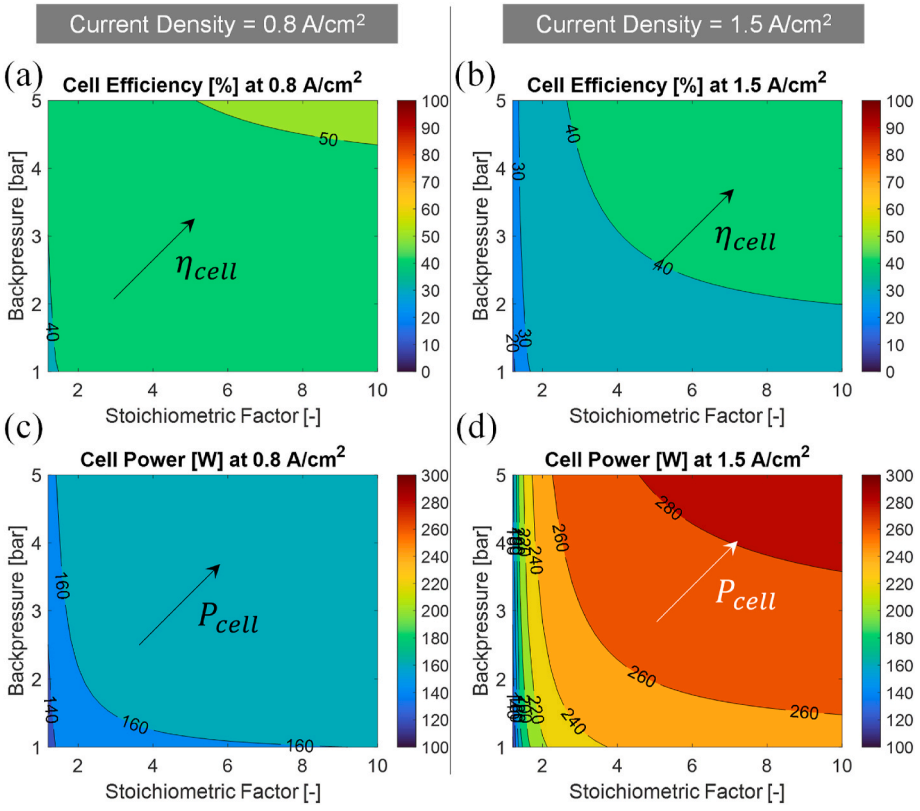

Fig. 3. Cell efficiency (top row, a-b, using Eq. (6)) and gross power (bottom row, c-d, using Eq. (7)) for MEA1 at $\boldsymbol{i = 0.8A/cm^2}$ (left column) and $\boldsymbol{i = 1.5A/\ cm^2}$ (right column).

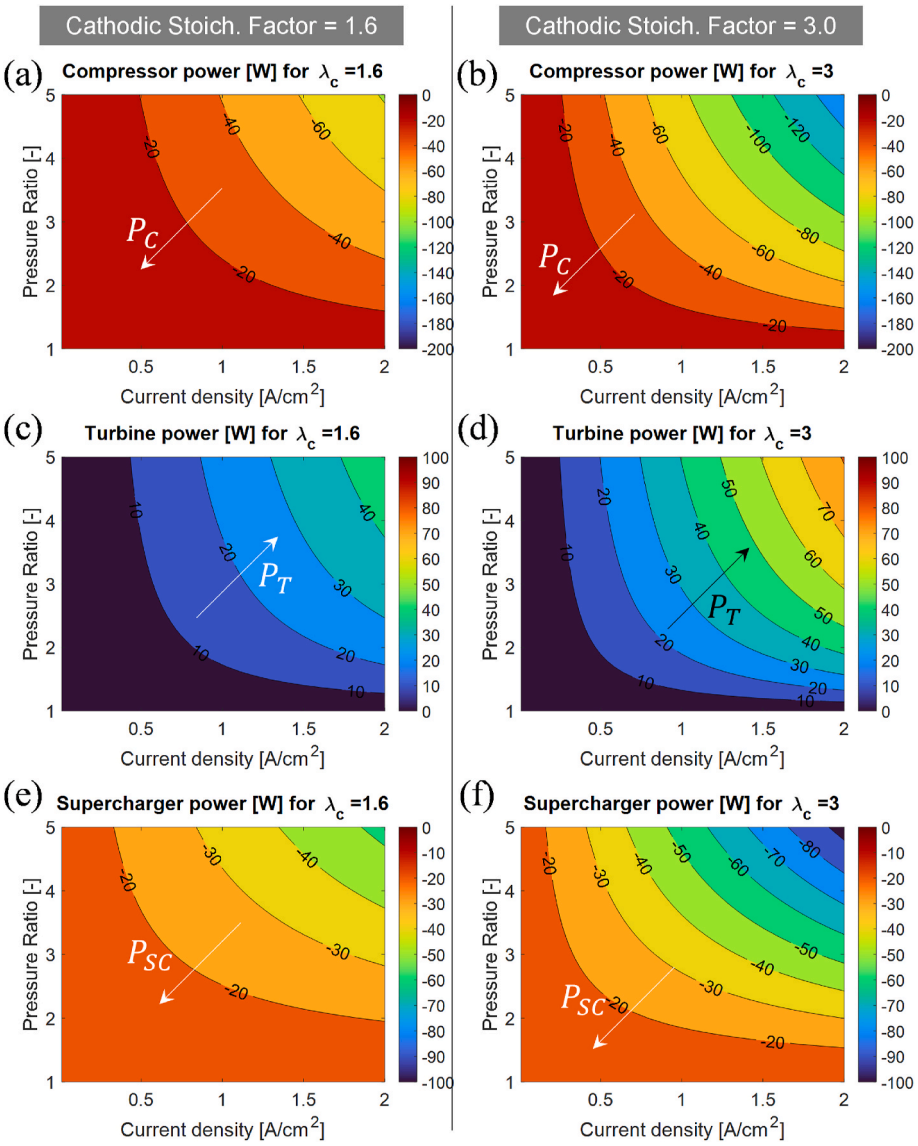

Fig. 4. Power contributions for compressor (top row, a-b, using Eq. (13)), turbine (middle row, c-d, using Eq. (19)) and supercharger (bottom row, e-f, using Eq. (20)) for the HE supercharging case at $\lambda_c = 1.6$ (left column) and $\lambda_c = 3.0$ (right column).

for the highest (p_c, λ_c) values (i.e., top-right corner). The supercharging power is reported in Fig. 4-e/f, confirming for all cases a net power request (negative values), and indicating the maximum demand for the highest (p_c, λ_c) values, which are critically the same conditions for optimal cell performance indicated in Fig. 3. Therefore, the analysis necessarily moves to the evaluation of the overall FCS, presented in the next section.

3.3. Results of FCS efficiency analysis

The net FCS efficiency (η_{FCS}) is obtained as in Eq. (23) for varying p_c and λ_c, and this is considered the single key value to maximize when designing an FCS. The respective influence of the operating parameters (p_c and λ_c) on the system efficiency is investigated from two different perspectives to identify:

- The (p_c,λ_c) ranges for maximum relative increase in η_{FCS}, with respect to the operation at minimal power demand (hereafter referred to as MPD), i.e. $\eta_{FCS,MPD}$ with $p_c^0 = 1.0\ bar$ and $\lambda_c^0 = 1.2$. The interest for this condition is motivated by the minimum power demand for supercharging (see Fig. 3), due to the absence of any air compression except that required to contrast the pressure losses in the cell flow (i.e., p_c equal to the ambient backpressure), and minimum flow rate for realistic operation ($\lambda_c = 1.2$). The relative variation in η_{FCS} is quantified with the $\eta_{FCS}^{\%}$ function as in Eq. (24), and it is used to select the (p_c, λ_c) ranges for maximum FCS efficiency relative gain. In view of the cost, weight, and added complexity of a supercharging system, this is believed to be a key indicator to quantify the convenience in introducing supercharging system under a given operating condition.

$$\eta_{FCS}^{\%}(p_c,\lambda_c) = \frac{\eta_{FCS}(p_c,\lambda_c) - \eta_{FCS,MPD}}{\eta_{FCS,MPD}}\ 100 \tag{24}$$

- The (p_c, λ_c) ranges for absolute maximum η_{FCS} values ($\eta_{FCS,max}$): this gives a different yet objective interpretation of the results, as a relevant increase in relative efficiency for a low-efficiency operation would equally result in a low-efficient FCS, thus marginally improving the global η_{FCS}. Therefore, the analysis is completed with the absolute η_{FCS} values.

The analysis will be presented in the next sections on four different cases, listed as:

- Case 1: MEA1 cell, HE supercharging.
- Case 2: MEA1 cell, LE supercharging.
- Case 3: MEA2 cell, HE supercharging.
- Case 4: MEA2 cell, LE supercharging.

3.3.1. FCS analysis for Case 1

The first analysis is carried out for Case 1 (MEA1 cell, HE supercharging) and in Fig. 5 the $\eta^{\%}_{FCS}(p_c, \lambda_c)$ field is reported for selected λ_c values to appreciate the relative gain/loss in the FCS efficiency with respect to the MPD condition. As clearly visible, for low-to-moderate λ_c (Fig. 5-a/b for $\lambda_c = 1.4/\ 2.0$, respectively), a relevant $\eta^{\%}_{FCS}$ gain is ubiquitously observed under all backpressure and currents, although it is accentuated for high current density due to the concentration overpotential reduction with respect to the flow rate at MPD ($\lambda^0_c = 1.2$). Moving to higher λ_c (Fig. 5-c/d for $\lambda_c = 4.0/\ 8.0$, respectively) the region of high $\eta^{\%}_{FCS}$ gain shrinks in the lower-right part of the graph (i.e., high current density and high backpressure), showing the emergence of (p_c, λ_c) conditions of negative $\eta^{\%}_{FCS}$, indicating a global penalty in FCS efficiency from the use of supercharging. This frames an antagonistic behaviour between (p_c, λ_c) for the system efficiency, with decreasing p_c necessary at higher λ_c and in line with the outcomes in Ref. [20]. Such outcomes open a crucial design decision whether to favour high flow rates (λ_c) rather than high cell pressure (p_c), and it shows the vastity of conditions for which a beneficial, yet sub-optimal, supercharging operation can be achieved with respect to the MPD condition (white-red areas in Fig. 5). However, a crucial need is the ability to *a priori* identify the (p_c, λ_c) values allowing the absolute maximum system efficiency using analytical tools, which is discussed in the next paragraph.

As it is re-emphasized that the results in Fig. 5 focus on the marginal gain and ignore the absolute η_{FCS} values, a second analysis investigates the (p_c, λ_c) values for maximum absolute η_{FCS}, and selected results are reported in Fig. 6 for the Case 1 at $i = 1.0 A/cm^2$, where the η_{FCS} values for both the MPD and ZG operations are indicated for the sake of comparison.

The considerations of the previous paragraph are found here in absolute terms, with operation at $\lambda_c \leq 3.0$ allowing to sustain pressure as high as $p_c > 5.0\ bar$ to obtain high η_{FCS}, consistently with the positive $\eta^{\%}_{FCS}$ field in Fig. 5-a, whereas moving to higher flow rates ($\lambda_c > 3.0$) requiring $p_c \leq 1.5\ bar$ to maximize η_{FCS}, in line with the outcomes in Refs. [14,17]. This confirms the anticipated antagonistic effect of λ_c and p_c on η_{FCS}. In Fig. 6 the scale is centred at the η_{FCS} of the MPD operation ($\eta_{FCS,MPD} = 0.29$) thus highlighting that:

- A wide range of generic (yet sub-optimal) η_{FCS} increase with respect to $\eta_{FCS,MPD}$ is present (light-red area), hence multiple (p_c, λ_c) choices would have led to some system efficiency gain in absence of a precise indication. Similar outcomes would have resulted if the ZG condition would have been chosen as a reference ($\eta_{FCS,ZG} = 0.31$). These are included as a reference and for metric purposes.
- The methodology indicates that the absolute maximum η_{FCS} ($\eta_{FCS,max} = 0.40$) is identified for $p_c = 1.2\ bar$ and $\lambda_c = 6.8$, confirming the dominant role of high flow rates alongside moderate supercharging level to optimize the net balance between higher power generation and power demand to optimize a FCS system efficiency. It is underlined that a wide area around the $\eta_{FCS,max}$ point is visible in Fig. 6, with $\eta_{FCS} > 0.39$, however confirming the high flow rate/low backpressure requirement for the air admission line, and whose generality will be expanded in the next section.

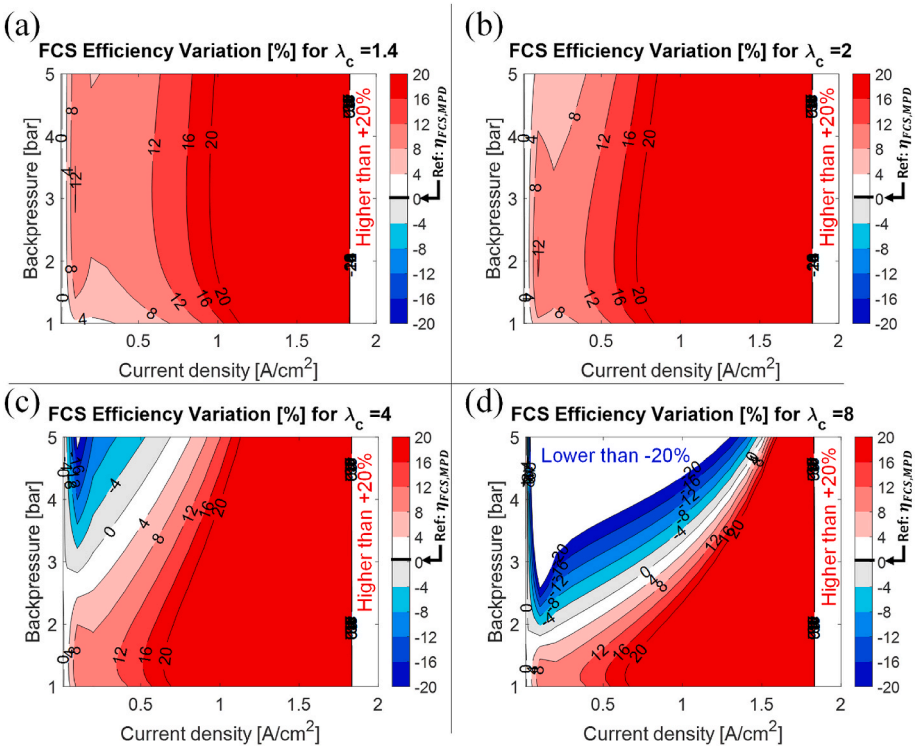

Fig. 5. Relative variation of FCS system efficiency ($\eta^{\%}_{FCS}$) for Case 1 (MEA1 cell, HE supercharging system), using Eq. (24): top left (a) for $\lambda_c = 1.4$, top right (b) for $\lambda_c = 2.0$, bottom left (c) for $\lambda_c = 4.0$ and bottom right (d) for $\lambda_c = 8.0$. The (i, λ_c) conditions for which $\eta^{\%}_{FCS}$ increase is higher than +4% with respect to the reference $\eta_{FCS,MPD}$ are in red shades, those for which $\eta^{\%}_{FCS}$ is almost identical (±4%) are in white/grey colours, and those for which $\eta^{\%}_{FCS}$ decrease is lower than −4% with respect to the reference $\eta_{FCS,MPD}$ are in blue shades. (For interpretation of the references to colour in this figure legend, the reader is referred to the Web version of this article.)

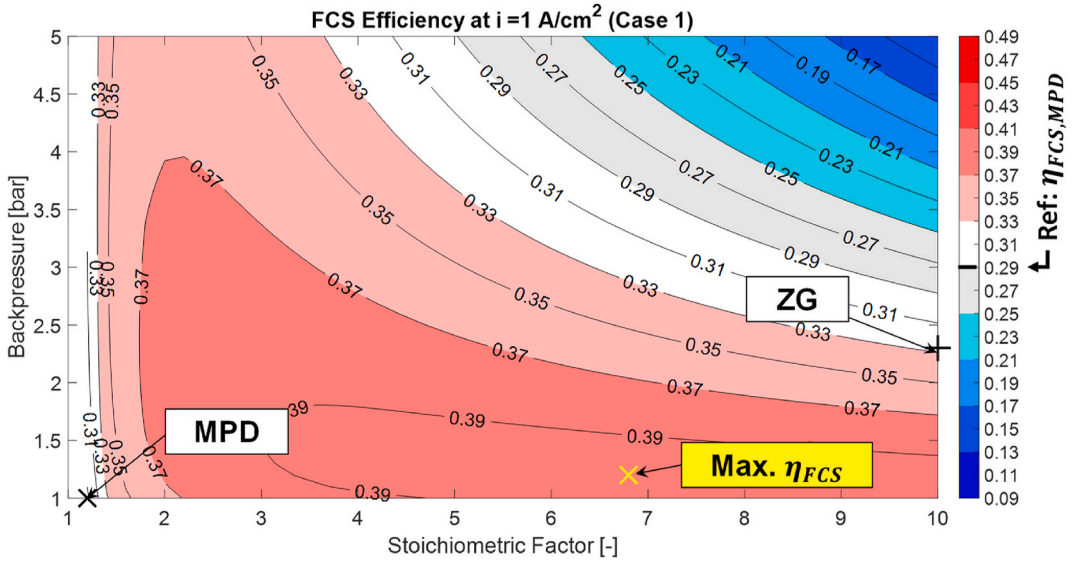

Fig. 6. FCS system efficiency (η_{FCS}) for Case 1 (MEA1 cell, HE supercharging system) at $\boldsymbol{i = 1.0A/cm^2}$, using Eq. (23). The colour scale is centred at the η_{FCS} of the MPD operation ($\eta_{FCS,MPD} = \mathbf{0.29}$) to facilitate comparisons. The (p_c,λ_c) conditions for which η_{FCS} increase is higher than +4% with respect to the reference $\eta_{FCS,MPD}$ are in red shades, those for which η_{FCS} is almost identical (±4%) are in white/grey colours, and those for which η_{FCS} decrease is lower than −4% with respect to the reference $\eta_{FCS,MPD}$ are in blue shades. (For interpretation of the references to colour in this figure legend, the reader is referred to the Web version of this article.)

3.3.2. FCS analysis for Case 2, 3, 4

The analysis on the objective identification of the maximum η_{FCS} is extended to Case 2, to evaluate the effect of LE supercharging machinery on the same MEA1 cell than in Case 1, and to Case 3 and 4, to analyse a FCS with a thinner membrane (MEA2) coupled with HE and LE supercharging.

The η_{FCS} fields are reported in Fig. 7 for Case 2 at $i = 1.0A/cm^2$, showing that the use of low-efficiency compressor and turbine leads to a dominant requirement to lower the cell operating pressure to ambient backpressure, indicating $\eta_{FCS,max} = 0.39$ for $p_c = 1.0\ bar$ and $\lambda_c = 6.4$. Clearly, the condition for maximum η_{FCS} is varied from that of Case 1, although still characterized by high flow rate/low backpressure.

The same analysis is extended to Case 3 and 4 at $i = 1.0A/cm^2$, using the MEA2 cell coupled with HE and LE equipment, respectively. The η_{FCS} fields are reported in Fig. 8-a/b, confirming the trend already seen for Case 1 and 2:

- When high-efficiency compressor and turbine are used (Case 3), the MEA2 cell allows $\eta_{FCS,max} = 0.44$ for $p_c = 1.3\ bar$ and $\lambda_c = 5.0$.
- In case of low-efficiency compressor and turbine (Case 4), the MEA2 cell can be optimized to $\eta_{FCS,max} = 0.43$ for $p_c = 1.0\ bar$ and $\lambda_c = 5.4$.

3.4. Effect of additional pressure losses

The presented results assumed that the compressor outlet pressure corresponded to the cell inlet one, i.e. that no additional pressure losses are present between compressor and PEMFC. However, in a real FCS several components might be present (e.g., intercooler, filter, humidi-

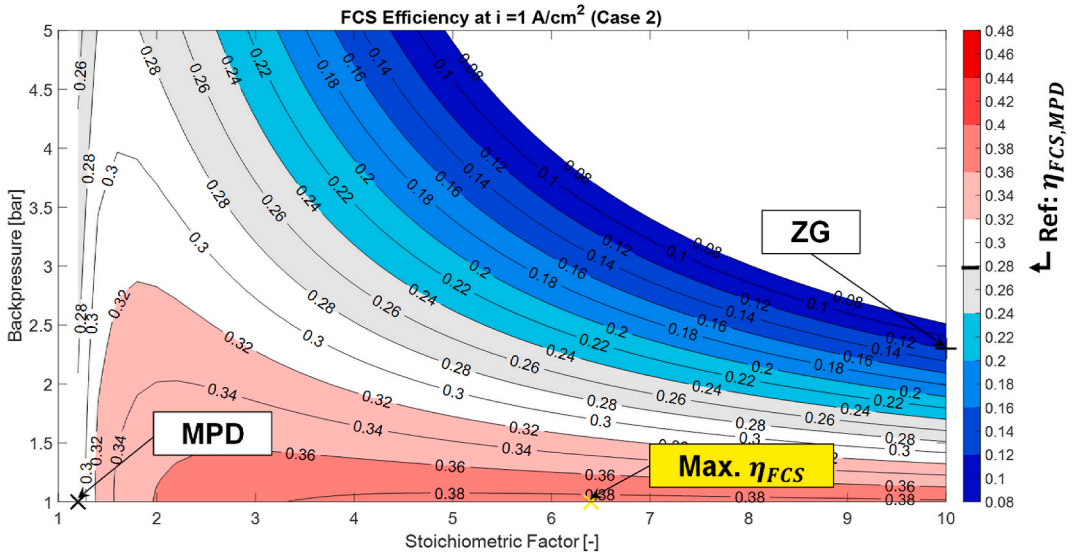

Fig. 7. FCS system efficiency (η_{FCS}) for Case 2 (MEA1 cell, LE supercharging system) at $\boldsymbol{i = 1.0A/cm^2}$, using Eq. (23). The colour scale is centred at the η_{FCS} of the MPD operation ($\eta_{FCS,MPD} = \mathbf{0.28}$) to facilitate comparisons. The (p_c,λ_c) conditions for which η_{FCS} increase is higher than +4% with respect to the reference $\eta_{FCS,MPD}$ are in red shades, those for which η_{FCS} is almost identical (±4%) are in white/grey colours, and those for which η_{FCS} decrease is lower than −4% with respect to the reference $\eta_{FCS,MPD}$ are in blue shades. (For interpretation of the references to colour in this figure legend, the reader is referred to the Web version of this article.)

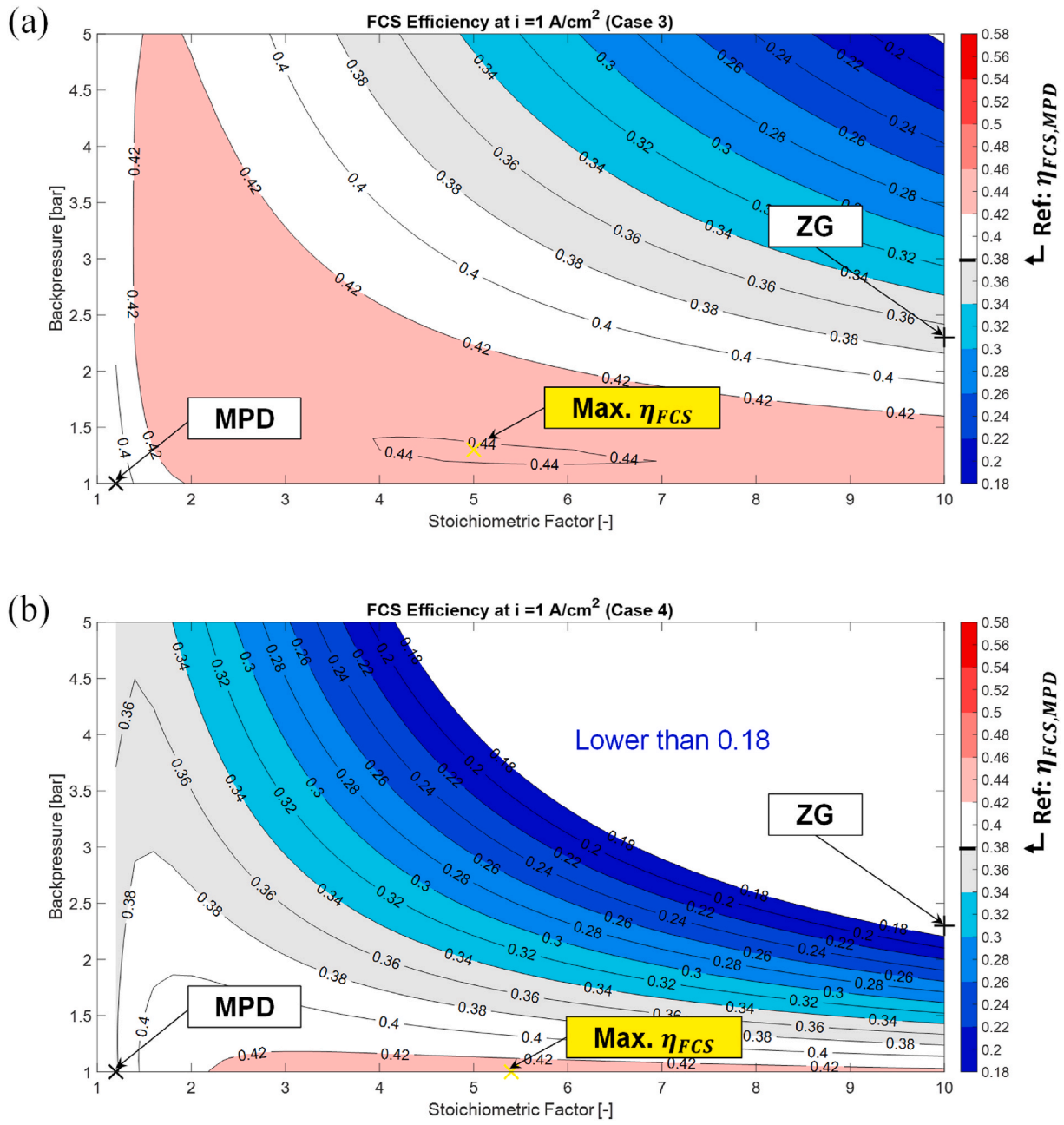

Fig. 8. FCS system efficiency (η_{FCS}) for (a) Case 3 (MEA2 cell, HE supercharging system) and (b) Case 4 (MEA2 cell, LE supercharging system) at $\boldsymbol{i = 1.0A/cm^2}$, using Eq. (23). The colour scales are centred at the η_{FCS} of the MPD operation ($\eta_{FCS,MPD} = \mathbf{0.39}$ for Case 3, $\eta_{FCS,MPD} = \mathbf{0.38}$ for Case 4) to facilitate comparisons. The (p_c,λ_c) conditions for which η_{FCS} increase is higher than +4% with respect to the reference $\eta_{FCS,MPD}$ are in red shades, those for which η_{FCS} is almost identical (±4%) are in white/grey colours, and those for which η_{FCS} decrease is lower than −4% with respect to the reference $\eta_{FCS,MPD}$ are in blue shades. (For interpretation of the references to colour in this figure legend, the reader is referred to the Web version of this article.)

fier, throttle valves, etc), introducing additional pressure losses to the air flow, as well as the distributed and concentration losses generated by the design of the air piping itself. In order to account for this, and to preserve the generality of the demonstration, the methodology for the optimal (p_c, λ_c) condition is applied introducing an additional pressure loss before the cell inlet, thus increasing the compressor outlet pressure for equal cell operating pressure. This term is modelled as a multiple of Eq. (9), bundling the same expression for the pressure losses used for the cell flow and preserving the formal dependency on the pipe length, diameter, and quadratic dependency on the flow velocity as a function of λ_c, as in Eq. (8). To mimic medium and high pressure losses, a multiplying factor is introduced ($K_{\Delta p}$) of 10 and 30 are used for Case 1, i.e. the air piping pressure losses between the compressor and the cell are 10 and 30 times the pressure losses in the cell itself, respectively. Fig. 9 shows the effect of such pressure losses on the (p_c, λ_c) values for $\eta_{FCS,max}$, indicating that:

- A substantial reduction of λ_c is observed from the reference value of $\lambda_c = 6.8$ (for no additional pressure losses, i.e. $K_{\Delta p} = 0$), to $\lambda_c = 3.8$ (for $K_{\Delta p} = 10$) and $\lambda_c = 3.0$ (for $K_{\Delta p} = 30$). The introduction of this additional pressure loss term leads to values for λ_c close to the experimentally reported in Refs. [14,17], requiring a simple measurement of air line pressure loss and still preserving the analytical formalism and a general applicability.

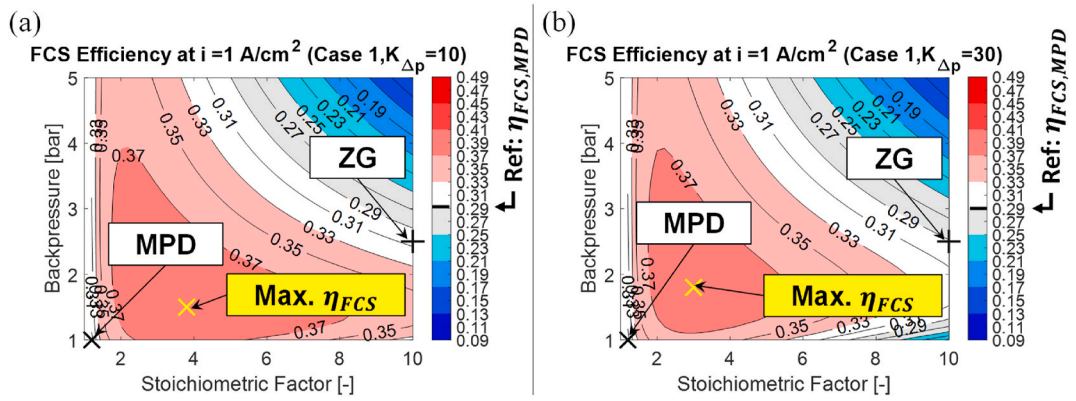

Fig. 9. Fig. 6. FCS system efficiency (η_{FCS}) for Case 1 (MEA1 cell, HE supercharging system) at $i = 1.0A/cm^2$, using Eq. 23, for $K_{\Delta p} = 10$ (a) and $K_{\Delta p} = 30$ (b). The colour scale is centred at the η_{FCS} of the MPD operation ($\eta_{FCS,MPD} = 0.28$) to facilitate comparisons. The (p_c,λ_c) conditions for which η_{FCS} increase is higher than +4% with respect to the reference $\eta_{FCS,MPD}$ are in red shades, those for which η_{FCS} is almost identical (±4%) are in white/grey colours, and those for which η_{FCS} decrease is lower than −4% with respect to the reference $\eta_{FCS,MPD}$ are in blue shades. (For interpretation of the references to colour in this figure legend, the reader is referred to the Web version of this article.)

- A marginal increase in p_c observed from the reference value of $p_c = 1.2$ (for no additional pressure losses, i.e. $K_{\Delta p} = 0$), to $p_c = 1.5$ (for $K_{\Delta p} = 10$) and $p_c = 1.8$ (for $K_{\Delta p} = 30$). This reinforces the indication that low-to-moderate pressure ratios are generally preferrable to maximize η_{FCS}.
- As expected, it is also observed that the absolute $\eta_{FCS,max}$ reduces for additional pressure losses from the reference value of $\eta_{FCS,max} = 0.40$ (for no additional pressure losses, i.e. $K_{\Delta p} = 0$), to $\eta_{FCS,max} = 0.395$ (for $K_{\Delta p} = 10$) and $\eta_{FCS,max} = 0.38$ (for $K_{\Delta p} = 30$).

3.5. Discussion of the results

The discussed results report the use of a unique methodology to analytically identify the optimal cathodic pressure and flow rate values (p_c, λ_c) to maximize the system efficiency (η_{FCS}) on four different cases at $i = 1.0A/cm^2$, where two PEMFCs (MEA1 and MEA2) are coupled with high- and low-efficiency supercharging systems (HE and LE). For each case, the identified maximum system efficiency ($\eta_{FCS,max}$) is compared with that obtained under the minimum power demand ($\eta_{FCS,MPD}$) and zero-gradient ($\eta_{FCS,ZG}$) conditions, and the comparison aims at demonstrating the generality of the methodology to any FCS. In Fig. 10 all the results are synthesized in the hypothesis of no pressure losses between the air compressor and the cell ($K_{\Delta p} = 0$), showing that the application of the presented method systematically increases the system efficiency with respect to both the MPD and ZG operation. Despite the arbitrary choice of MPD and ZG for system efficiency analyses, Figs. 6–8 unambiguously show the generality of the methodology and the absolute maximum of $\eta_{FCS,max}$, hence it maximizes the FCS efficiency independently of the reference condition (MPD and ZG, in this study). Moreover, the variation of cell and supercharging equipment from Cases 1 to 4 allows to draw a rather general indication for high flow rates ($\lambda_c = 5.0 - 6.8$) and low backpressure ($p_c = 1.0 - 1.3$ *bar*) to maximize η_{FCS}, in line with the outcomes in Refs. [20–22] and with exact values depending on the specific case. This is further generalized when the pressure losses between the air compressor and the cell inlet are included, here exemplified by the $K_{\Delta p} = 10$ and $K_{\Delta p} = 30$ cases. The analysis shown in Fig. 9 is repeated for all the cases and the results are reported in Fig. 11, confirming that the λ_c leading to $\eta_{FCS,max}$ lowers ($\lambda_c = 2.2 - 3.0$), whereas the cell backpressure slightly increases ($p_c = 1.2 - 2.0$ *bar*). Such results reinforce the primary goal of minimizing the pressure losses not only in the cell flow, but in the entire air line, to maximize the system efficiency using high flow rates and low pressure ratios. In case this is not possible due to design constraints, a different optimum (p_c, λ_c) point is identified at reduced flow rate and higher pressure ratio, and the entity of both variations is calculated based on a simple pressure drop measurement of the air supply line, whose effect is included in the presented methodology. These outcomes and the analytical derivation of the methodology are considered of high relevance to maximize the efficiency of FCS, and the developed MATLAB script will be made available upon request to the authors under the FAIR (Findable, Accessible, Interoperable, Reusable) guidelines.

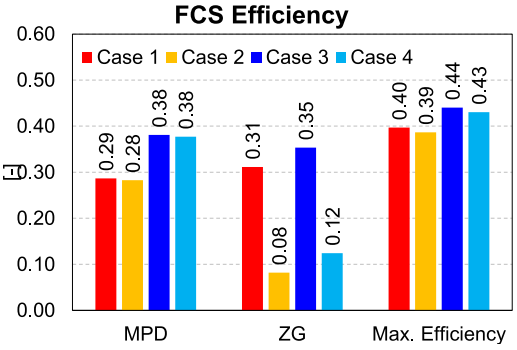

Fig. 10. FCS efficiency at $i = 1.0A/cm^2$ for the minimum power demand (MPD), zero-gradient operation (ZG) and maximum efficiency conditions for Cases 1–4 under the hypothesis of no additional pressure loss between the air compressor and the cell ($K_{\Delta p} = 0$).

4. Conclusions

In this study an analytical methodology is proposed to objectively evaluate the efficiency variation in operating fuel cell systems at high pressure and/or flow rates using supercharging systems, here evaluated via the cell backpressure (p_c) and the stoichiometric flow rate (λ_c). Both factors affect in a complex way both the power generation in the cell, where they should be jointly increased, and the power demand of the supercharger, where a minimization of both would be beneficial. This opens the design choice to favour p_c rather than λ_c for maximum system efficiency (η_{FCS}), and despite multiple analyses are present in the specialized literature, their contradictory indications and the lack of a unified explanation have created a field of design indecision in terms of optimal (p_c, λ_c). Therefore, in this study an analytical methodology is devised to *a priori* evaluate the best-efficiency conditions for maximum η_{FCS} ($\eta_{FCS,max}$), and steady-state conditions are evaluated on a typical PEMFC system spanning a wide band of pressure levels ($p_c = 1.0 -$

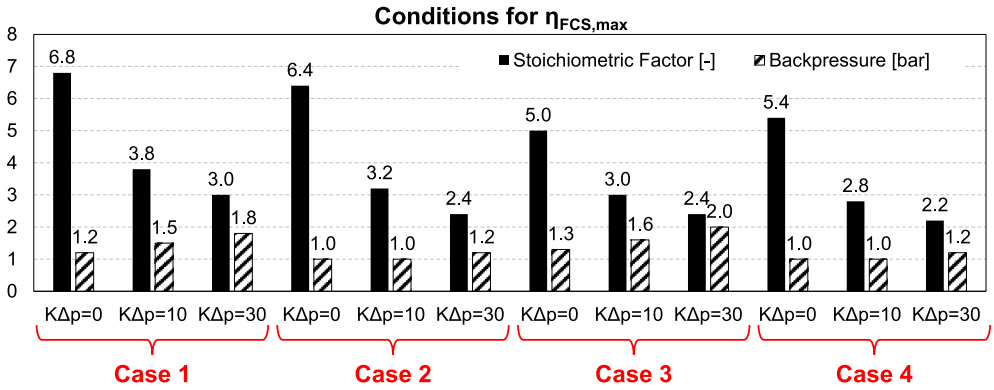

Fig. 11. (p_c, λ_c) values for $\eta_{FCS,max}$ for Cases 1 to 4 (from left to right), under the hypotheses of no additional pressure loss between air compressor and cell ($K_{\Delta p} = 0$), and with increasing pressure losses ($K_{\Delta p} = 10$ and $K_{\Delta p} = 30$).

5.0 *bar*) and air flow rates ($\lambda_c = 1.2 - 10.0$). A demonstration study is carried out on two membrane and electrode assemblies (MEA1 and MEA2) tested at Joint Research Centre and documented in Refs. [24,25], coupled to both a high- and a low-efficiency compressor and turbine. The matrix of four cases is examined for varying (p_c, λ_c) and the conditions for $\eta_{FCS,max}$ are identified. The results show that:

- The operation at low-to-moderate cell backpressure is the primary factor to maximize η_{FCS}. For both MEA1 and MEA2 cells, when coupled with high-efficiency compressor and turbine a moderate backpressure ($p_c = 1.2 - 1.3\ bar$) is beneficial. However, in case their efficiency is low the operation at ambient backpressure ($p_c = 1.0\ bar$) is mandatory to maximize η_{FCS}.
- High stoichiometric factors (in the range $\lambda_c = 5.0 - 6.8$) are recommended to maximize η_{FCS} in case of minimum or null pressure losses between the air compressor and the cell inlet, at least for parallel channel flow fields where pressure losses remain moderate and the flow regime laminar.
- When the pressure losses in the air line are included, the same methodology indicates a lower stoichiometric ratio ($\lambda_c = 2.2 - 3.0$) and a slightly higher cell backpressure ($p_c = 1.2 - 2.0\ bar$).
- The model-guided selection of p_c and λ_c using the methodology presented in this study allows to unambiguously identify the (p_c, λ_c) values for $\eta_{FCS,max}$. This is confirmed by the fields of η_{FCS} for all the four cases (Figs. 6–8).
- The use of extremely high flow rates is at best ineffective, having a moderate influence on $\eta_{FCS,max}$ when operating at low p_c values. Conversely, a severe efficiency penalty arises for higher p_c values, discouraging such practice.

The obtained results demonstrate how the presented methodology could be applied to any cell and supercharging system to *a priori* identify the optimal (p_c, λ_c) for $\eta_{FCS,max}$. The generality is guaranteed by the analytical derivation based on power balances, allowing to include the impact of pressure losses in the air admission line. The obtained conclusions reinforce the primary indication of moderate-to-low backpressure operation, typical of parallel channel flow fields, alongside high flow rates as the conditions for $\eta_{FCS,max}$. This is believed to be a relevant advancement in the field of FCS design and engineering, in view of the rigorous derivation and conclusions and with profound design implications. The model has been implemented in a MATLAB script which will be made available upon request to the authors under the FAIR (Findable, Accessible, Interoperable, Reusable) guidelines, and which candidates to be incorporated in industrial-grade R&D workflows to guide the selection of the best components for the air admission line, thus enhancing the advancement in fuel cells engineering.

CRediT authorship contribution statement

Alessandro d'Adamo: Writing – original draft, Supervision, Project administration, Methodology, Investigation, Funding acquisition, Formal analysis, Data curation, Conceptualization. **Lorenzo Martoccia:** Writing – review & editing, Methodology, Investigation, Funding acquisition. **Fabio Berni:** Writing – review & editing, Visualization, Methodology, Investigation. **Sebastiano Breda:** Investigation, Funding acquisition, Data curation.

Declaration of competing interest

The authors declare the following financial interests/personal relationships which may be considered as potential competing interests: Alessandro d'Adamo reports financial support was provided by European Union, NextGenerationEU - National Sustainable Mobility Center - MOST, CN00000023, Italian Ministry of University and Research, Spoke 12 (CUP E93C22001070001). Sebastiano Breda reports financial support was provided by European Union, NextGenerationEU - National Sustainable Mobility Center - MOST, CN00000023, Italian Ministry of University and Research, Spoke 12 (CUP E93C22001070001). Lorenzo Martoccia reports financial support was provided by Regione Emilia-Romagna (Italy), Borsa di Dottorato (39 ciclo). Fabio Berni acknowledges the financial support provided by the Dipartimento di Ingegneria "Enzo Ferrari" (Università degli Studi di Modena e Reggio Emilia), under the FAR Dipartimentale 2024-25 project.

Acknowledgement

Alessandro d'Adamo and Sebastiano Breda acknowledge the financial support provided by European Union, NextGenerationEU - National Sustainable Mobility Center - MOST, CN00000023, Italian Ministry of University and Research, Spoke 12 (CUP E93C22001070001). Lorenzo Martoccia acknowledges the financial support provided by Regione Emilia-Romagna (Italy), Borsa di Dottorato (39 ciclo). Fabio Berni acknowledges the financial support provided by the Dipartimento di Ingegneria "Enzo Ferrari" (Università degli Studi di Modena e Reggio Emilia), under the FAR Dipartimentale 2024-25 project.

References

[1] Larminie J, Dicks A. Fuel cell systems explained. Fuel cell systems explained. second ed. Dec. 2013. p. 1–406. https://doi.org/10.1002/9781118878330. Second Edition.
[2] Barbir F. PEM fuel cells : theory and practice. 2013. p. 518.
[3] Wang Y, Chen KS, Mishler J, Cho SC, Adroher XC. A review of polymer electrolyte membrane fuel cells: technology, applications, and needs on fundamental research. Appl Energy Apr. 2011;88(4):981–1007. https://doi.org/10.1016/J.APENERGY.2010.09.030.

[4] World energy outlook 2023 – analysis - IEA [Online], https://www.iea.org/reports/world-energy-outlook-2023. [Accessed 27 February 2024].
[5] Qasem NAA. A recent overview of proton exchange membrane fuel cells: fundamentals, applications, and advances. Appl Therm Eng Sep. 2024;252:123746. https://doi.org/10.1016/J.APPLTHERMALENG.2024.123746.
[6] Shahzad K, Iqbal Cheema I. Low-carbon technologies in automotive industry and decarbonizing transport. J Power Sources Jan. 2024;591:233888. https://doi.org/10.1016/J.JPOWSOUR.2023.233888.
[7] Agyekum EB, Odoi-Yorke F, Abbey AA, Ayetor GK. A review of the trends, evolution, and future research prospects of hydrogen fuel cells – a focus on vehicles. Int J Hydrogen Energy Jun. 2024;72:918–39. https://doi.org/10.1016/J.IJHYDENE.2024.05.480.
[8] Aminudin MA, Kamarudin SK, Lim BH, Majilan EH, Masdar MS, Shaari N. An overview: current progress on hydrogen fuel cell vehicles. Int J Hydrogen Energy Feb. 2023;48(11):4371–88. https://doi.org/10.1016/J.IJHYDENE.2022.10.156.
[9] Pramuanjaroenkij A, Kakaç S. The fuel cell electric vehicles: the highlight review. Int J Hydrogen Energy Mar. 2023;48(25):9401–25. https://doi.org/10.1016/J.IJHYDENE.2022.11.103.
[10] Wang CY. Fundamental models for fuel cell engineering. Chem Rev Oct. 2004;104(10):4727–65. https://doi.org/10.1021/CR020718S.
[11] Jiao K, Li X. Water transport in polymer electrolyte membrane fuel cells. Prog Energy Combust Sci Jun. 2011;37(3):221–91. https://doi.org/10.1016/J.PECS.2010.06.002.
[12] Kerviel A, et al. An evaluation of turbocharging and supercharging options for high-efficiency fuel cell electric vehicles. Appl Sci 2018;8:2474. https://doi.org/10.3390/APP8122474. vol. 8, no. 12, p. 2474, Dec. 2018.
[13] Sugawara T, Kanazawa T, Imai N, Tachibana Y. Development of motorized turbo compressor for clarity fuel cell. SAE technical papers, 2017-March; March, Mar. 2017. https://doi.org/10.4271/2017-01-1187.
[14] Lu JB, Wei GH, Zhu FJ, Yan XH, Zhang JL. Pressure effect on the PEMFC performance. Fuel Cell Jun. 2019;19(3):211–20. https://doi.org/10.1002/FUCE.201800135.
[15] Santarelli MG, Torchio MF. Experimental analysis of the effects of the operating variables on the performance of a single PEMFC. Energy Convers Manag Jan. 2007;48(1):40–51. https://doi.org/10.1016/J.ENCONMAN.2006.05.013.
[16] Wang L, Husar A, Zhou T, Liu H. A parametric study of PEM fuel cell performances. Int J Hydrogen Energy Nov. 2003;28(11):1263–72. https://doi.org/10.1016/S0360-3199(02)00284-7.
[17] Kim HS, Lee DH, Min K, Kim M. Effects of key operating parameters on the efficiency of two types of PEM fuel cell systems (high-pressure and low-pressure operating) for automotive applications. J Mech Sci Technol 2005;19(4):1018–26. https://doi.org/10.1007/BF02919185/METRICS.
[18] Hoeflinger J, Hofmann P. Air mass flow and pressure optimisation of a PEM fuel cell range extender system. Int J Hydrogen Energy Oct. 2020;45(53):29246–58. https://doi.org/10.1016/J.IJHYDENE.2020.07.176.
[19] Qin Y, Du Q, Fan M, Chang Y, Yin Y. Study on the operating pressure effect on the performance of a proton exchange membrane fuel cell power system. Energy Convers Manag Jun. 2017;142:357–65. https://doi.org/10.1016/J.ENCONMAN.2017.03.035.
[20] Chen H, Liu B, Liu R, Weng Q, Zhang T, Pei P. Optimal interval of air stoichiometry under different operating parameters and electrical load conditions of proton exchange membrane fuel cell. Energy Convers Manag Feb. 2020;205:112398. https://doi.org/10.1016/J.ENCONMAN.2019.112398.
[21] Martinez-Boggio S, Di Blasio D, Fletcher T, Burke R, García A, Monsalve-Serrano J. Optimization of the air loop system in a hydrogen fuel cell for vehicle application. Energy Convers Manag May 2023;283:116911. https://doi.org/10.1016/J.ENCONMAN.2023.116911.
[22] Santarelli MG, Torchio MF, Calì M, Giaretto V. Experimental analysis of cathode flow stoichiometry on the electrical performance of a PEMFC stack. Int J Hydrogen Energy May 2007;32(6):710–6. https://doi.org/10.1016/J.IJHYDENE.2006.08.008.
[23] Ge X, Li K, Tian W, Wang R, Wan X, Tang H. Efficiency improvement strategy of fuel cell system based on oxygen excess ratio and cathode pressure two-dimensional optimization. Int J Hydrogen Energy Feb. 2024;57:136–47. https://doi.org/10.1016/J.IJHYDENE.2023.12.294.
[24] Bednarek T, Tsotridis G. Development of reference hardware for a harmonised testing of PEM single cell fuel cells - publications Office of the EU [Online], https://op.europa.eu/en/publication-detail/-/publication/57794ea3-7585-11eb-9ac9-01aa75ed71a1/language-en. [Accessed 30 April 2024].
[25] Bednarek T, Tsotridis G. Assessment of the electrochemical characteristics of a Polymer Electrolyte Membrane in a reference single fuel cell testing hardware. J Power Sources Oct. 2020;473:228319. https://doi.org/10.1016/J.JPOWSOUR.2020.228319.
[26] Kulikovsky AA. The voltage–current curve of a polymer electrolyte fuel cell: 'exact' and fitting equations. Electrochem Commun Nov. 2002;4(11):845–52. https://doi.org/10.1016/S1388-2481(02)00466-6.
[27] Kulikovsky AA. The effect of stoichiometric ratio λ on the performance of a polymer electrolyte fuel cell. Electrochim Acta Feb. 2004;49(4):617–25. https://doi.org/10.1016/J.ELECTACTA.2003.09.016.
[28] Corda G, Cucurachi A, Diana M, Fontanesi S, D'Adamo A. A methodology to design the flow field of PEM fuel cells. Apr. 2023. https://doi.org/10.4271/2023-01-0495.
[29] Li X, Sabir I, Park J. A flow channel design procedure for PEM fuel cells with effective water removal. J Power Sources Jan. 2007;163(2):933–42. https://doi.org/10.1016/J.JPOWSOUR.2006.10.015.
[30] Cengel Yunus A, Dall'O' Giuliano, Sarto Luca. Termodinamica E trasmissione del calore 5/ED [Online]. Available: https://www.mheducation.it/termodinamica-e-trasmissione-del-calore-5-ed-con-connect-9788838655630-italy. [Accessed 30 September 2022].
[31] Janssen GJM, Overvelde MLJ. Water transport in the proton-exchange-membrane fuel cell: measurements of the effective drag coefficient. J Power Sources Oct. 2001;101(1):117–25. https://doi.org/10.1016/S0378-7753(01)00708-X.
[32] Thomas A, Maranzana G, Didierjean S, Dillet J, Lottin O. Heat fluxes and electrodes temperature in a proton exchange membrane fuel cell. Mechanics & Industry 2012;13(4):255–60. https://doi.org/10.1051/MECA/2012021.